Published in final edited form as:
Gut. 2014 December ; 63(12): 1960–1971. doi:10.1136/gutjnl-2013-306294.

CCL2-dependent infiltrating macrophages promote angiogenesis in progressive liver fibrosis

Josef Ehling[#1,2], **Matthias Bartneck**[#3], **Xiao Wei**[3], **Felix Gremse**[1], **Viktor Fech**[3], **Diana Möckel**[1], **Christer Baeck**[3], **Kanishka Hittatiya**[4], **Dirk Eulberg**[5], **Tom Luedde**[3], **Fabian Kiessling**[1], **Christian Trautwein**[3], **Twan Lammers**[1,6,7,*], and **Frank Tacke**[3,*]

[1]Department of Experimental Molecular Imaging, Helmholtz Institute for Biomedical Engineering, Medical Faculty, RWTH University, Aachen, Germany [2]Institute of Pathology, Medical Faculty, RWTH University, Aachen, Germany [3]Department of Medicine III, Medical Faculty, RWTH University, Aachen, Germany [4]Institute of Pathology, University Bonn, Bonn, Germany [5]NOXXON Pharma AG, Berlin, Germany [6]Department of Targeted Therapeutics, MIRA Institute for Biomedical Technology and Technical Medicine, University of Twente, Enschede, The Netherlands [7]Department of Pharmaceutics, Utrecht Institute for Pharmaceutical Sciences, Utrecht University, Utrecht, The Netherlands

[#] These authors contributed equally to this work.

Abstract

Objectives—In chronic liver injury, angiogenesis, the formation of new blood vessels from pre-existing ones, may contribute to progressive hepatic fibrosis and to development of hepatocellular carcinoma. Although hypoxia-induced expression of vascular endothelial growth factor (VEGF) occurs in advanced fibrosis, we hypothesized that inflammation may endorse hepatic angiogenesis already at early stages of fibrosis.

Design—Angiogenesis in livers of c57BL/6 mice upon carbon tetrachloride (CCl_4) or bile duct ligation (BDL) induced chronic hepatic injury was non-invasively monitored using *in vivo* contrast-enhanced micro-computed tomography (CT) and *ex vivo* anatomical μCT after hepatic Microfil perfusion. Functional contributions of monocyte-derived macrophage subsets for angiogenesis were explored by pharmacological inhibition of CCL2 using the Spiegelmer mNOX-E36.

Results—Contrast-enhanced *in vivo* μCT imaging allowed non-invasively monitoring the close correlation of angiogenesis, reflected by functional hepatic blood vessel expansion, with experimental fibrosis progression. On a cellular level, inflammatory monocyte-derived

[*]**Address for correspondence:** Prof. Dr. Dr. Frank Tacke, Department of Medicine III, Medical Faculty of the RWTH Aachen, Pauwelsstr. 30, 52074 Aachen, Germany, Phone: +49-241-8035101, Fax: +49-241-8082455, frank.tacke@gmx.net; Dr. Dr. Twan Lammers, Department of Experimental Molecular Imaging, Medical Faculty of the RWTH Aachen, Pauwelsstr. 30, 52074 Aachen, Germany, Phone: +49-241-8080116, Fax: +49-241-8082006, tlammers@ukaachen.de.

Contributors: J.E., M.B., X.W., F.G., V.F. and D.M. performed experiments, acquired data and analyzed results; C.B. and D.E. contributed methodology for CCL2 inhibition; K.H. performed immunohistochemistry and analyzed results; T.L., F.K. and CT helped in data interpretation and provided important intellectual content; J.E., M.B., T.L. and F.T. designed the study, analyzed data and wrote the manuscript.

Competing interest: Dirk Eulberg is an employee of Noxxon Pharma AG. All other authors have nothing to disclose.

Europe PMC Funders Author Manuscripts

macrophages massively accumulated in injured livers, co-localized with newly formed vessels in portal tracts and exhibited pro-angiogenic gene profiles including up-regulated VEGF and MMP9. Functional *in vivo* and anatomical *ex vivo* μCT analyses demonstrated that inhibition of monocyte infiltration by targeting the chemokine CCL2 prevented fibrosis-associated angiogenesis, but not fibrosis progression. Monocyte-derived macrophages primarily fostered sprouting angiogenesis within the portal vein tract. Portal vein diameter as a measure of portal hypertension depended on fibrosis, but not on angiogenesis.

Conclusions—Inflammation-associated angiogenesis is promoted by CCL2-dependent monocytes during fibrosis progression. Innovative *in vivo* μCT methodology can accurately monitor angiogenesis and anti-angiogenic therapy effects in experimental liver fibrosis.

Keywords

liver fibrosis; angiogenesis; monocytes; computed tomography; chemokines

Introduction

Liver disease progression is accompanied by pathological angiogenesis [1, 2, 3], which is likely a prerequisite favouring development of hepatocellular carcinoma (HCC). However, although pathological angiogenesis is commonly observed in advanced fibrosis, it is currently unclear, if and how angiogenesis and fibrosis are linked during progression of chronic liver diseases [4]. Interestingly, anti-angiogenic multikinase inhibitors have demonstrated anti-fibrotic potential in preclinical settings [3, 5], and pro-inflammatory and pro-angiogenic factors are assumed to favour vessel sprouting, resulting in microstructural vascular changes and an increased intrahepatic vascular resistance [6]. Whereas several studies have reported that in late-stage liver fibrosis or cirrhosis the hypoxia-induced release of pro-angiogenic factors like vascular endothelial growth factor (VEGF) play an important role in the development of HCC [6, 7], only few studies have investigated the role of inflammatory cells in mediating angiogenesis associated with HCC [8, 9], non-alcoholic steatohepatitis [10] or cirrhosis [3]. Based on the pivotal role that (M2-polarized) macrophages play in tumor angiogenesis [11], we hypothesized that macrophages are key mediators of fibrosis-associated angiogenesis as well.

The macrophage pool of the liver is composed of resident immune cells, traditionally termed Kupffer cells, and infiltrating monocytes. In case of liver injury, bone marrow-derived monocytes massively accumulate in injured liver and differentiate into inflammatory macrophages, dependent on interactions of the chemokine receptor CCR2 with its ligand CCL2 [12, 13]. These infiltrating monocytes are characterized by the surface marker Ly-6C (Gr1) and a pro-inflammatory cytokine expression profile [14, 15], while expression of angiogenic factors has not been systematically addressed to date. We therefore aimed at investigating if inflammatory macrophages promote fibrosis-associated angiogenesis and, consequently, if the inhibition of monocyte migration into the liver results in a reduced angiogenic activity in chronically injured livers.

In spite of this, no efficient *in vivo* imaging techniques are currently established, neither for non-invasively quantifying fibrosis-associated pathological angiogenesis, nor for monitoring

Europe PMC Funders Author Manuscripts

therapy effects of novel pharmacological treatments in (pre-)clinical settings. At present, anti-angiogenic treatment effects are usually assessed by quantifying CD31-positive vascular structures using immunohistochemistry (IHC), and increased $CD31^+$ areas are also observed in virtually all types of advanced hepatic diseases in liver biopsies from human patients [2]. Though useful, this methodology does not allow longitudinal examinations during disease progression or quantifications of functional parameters such as blood volume, blood flow and tissue perfusion. In contrast, due to its high spatial resolution, its user-independency and its suitability for high-throughput analyses, (micro-)computed tomography (μCT) has become a (pre-)clinically relevant diagnostic modality for the non-invasive visualization and quantification of functional blood vessels [16]. The aim of this study was to establish novel μCT-based imaging protocols to characterize the role of CCL2-dependent inflammatory monocytes in mediating pathological angiogenesis during the initiation and progression of liver fibrosis. Alterations in the hepatic rBV as well as changes in the microarchitecture of liver blood vessels were visualized and quantified using functional *in vivo* μCT and anatomical *ex vivo* μCT, convincingly demonstrating that CCL2-dependent inflammatory monocyte-derived macrophages control angiogenesis in experimental liver fibrogenesis in mice.

Materials and Methods

Liver injury models and pharmacological CCL2 inhibition in mice

C57bl/6 wild-type mice were housed in a specific pathogen-free environment under ethical conditions approved by German legal requirements. Chronic liver injury was induced in 8-12 weeks old C57bl/6 wild-type mice by repetitive carbon tetrachloride (CCl_4) administration (0.6 ml/kg body weight) or by surgical ligation of the biliary duct (BDL), as described earlier [17]. To block CCL2-dependent monocyte migration, mice were treated with PEGylated L-RNA Spiegelmer mNOX-E36 (50 nucleotides long L-RNA oligonucleotide; 5′-GGC-GAC-AUU-GGU-UGG-GCA-UGA-GGC-GAG-GCC-CUU-UGA-UGA-AUC-CGC-GGC-CA-3′, 40kDa PEG), kindly provided by NOXXON Pharma AG (Berlin, Germany), subcutaneously three times per week at 20mg/kg body weight. mNOX-E36 binds specifically to murine CCL2 (MCP-1) and inhibits its biological effects *in vitro* and *in vivo* [12]. Liver injury, fibrosis progression and immune cell alterations were assessed as published earlier [12, 17]. Primary hepatocytes were isolated by conventional methodology, all other primary cell types (stellate cells, endothelial cells, Kupffer cells, inflammatory macrophages) after collagenase/pronase-perfusion, gradient centrifugation and ultrapure FACS sorting using a BD Aria SORP equipped with an UV laser [18]. Details on methodology are provided as online supplementary methods.

In vivo micro-computed tomography

For contrast-enhanced *in vivo* μCT imaging, a dual-energy flat-panel micro-computed tomography scanner was employed (TomoScope 30s Duo; CT Imaging, Erlangen, Germany). Mice were scanned before and immediately after i.v. injection of 100 μl eXIA™160XL (Binitio Biomedical, Ottawa, Canada), an iodine-based blood pool contrast agent optimized for *in vivo* μCT. Animals were anesthetized with 1.5% isoflurane in oxygen-enriched air during the entire *in vivo* imaging process. For each mouse, a dual-

energy scan was performed at 41 and 65 kV (at 0.5 mA and 1 mA), acquiring 2880 projections of size 1032×1024 over 6 minutes of continuous rotation for each tube. A Feldkamp-type reconstruction algorithm (CT-Imaging, Erlangen, Germany) was implemented with a voxel size of $35\times35\times35\mu m^3$, including ring artefact correction. The reconstructed data were visualized and analyzed with Imalytics Preclinical software (Philips Research, Aachen, Germany)[19]. After 3D liver segmentation, which was performed by interactively delineating the liver boundaries in 10-20 slices, rBV values were determined based on the mean brightness of the liver after contrast agent injection, a large blood vessel after contrast agent injection (100% rBV) and the liver before contrast agent administration (0% rBV) [20]. Portal vein diameter was quantified on cross-sectional images in transversal planes 3-4 slices above the junction of the superior mesenteric and splenic vein [21].

Ex vivo micro-computed tomography

After *in vivo* μCT imaging, mice were intracardially perfused with Microfil (Flow Tech, Carver, MA, USA), a lead-containing silicone rubber CT contrast agent for high-resolution 3D investigation of the microarchitecture of blood vessels in the liver. Microfil replaces the blood volume and polymerizes intravascularly 20 minutes after application, resulting in vascular casting. Perfusion was performed by direct infusion of Microfil into the left ventricle (after incising the inferior vena cava) at physiological pressures by using a perfusion pump. After Microfil perfusion and solidification of the contrast medium, the liver was excised, formalin-fixed and scanned using a high-resolution SkyScan 1172 μCT system (SkyScan, Kontich, Belgium). Livers were positioned on a computer-controlled rotation platform and scanned 180° around the vertical axis in rotation steps of 0.3° at 100 kV and an electric current of 100 μA, resulting in 640 acquired projections (4000×2096 pixels). Acquisition times for whole livers ranged from 6-8 h. Reconstructions of a voxel size of $6\times6\times6\mu m^3$ were performed using filtered backprojection (Feldkamp-type). The volume data was downsampled to a voxel size of $12\times12\times12\mu m^3$ for image processing. After 3D volume rendering of reconstructed high-resolution μCT data sets, blood vessel branching and 3D micromorphology of vessels were systematically and semi-automatically analyzed, using Imalytics Preclinical software. For this approach, 5 representative vessels were analyzed, and the number of blood vessel branches per primary vessel was quantified in total and relatively per rising branching order.

Results

Angiogenesis, but not inflammation, correlates closely with progressive fibrosis in chronic liver injury

In order to delineate the association between progressive liver injury, inflammation, fibrosis and angiogenesis, chronic toxic liver injury was induced by repetitive (twice weekly) injections of carbon tetrachloride (CCl_4) in c57bl/6 wildtype mice. After 2, 4, 6 and 8 weeks, a progressive liver damage including necrotic areas, characteristic fibrotic bridging, infiltration of $CD45^+$ leukocytes and formation of new $CD31^+$ hepatic blood vessels was observed (Fig.1A). Interestingly, the kinetics between these principal features differed considerably: while liver cell injury as reflected by ALT activity in serum remained stably elevated throughout the time-course of repetitive CCl_4 injections, the infiltration of $CD45^+$

leukocytes into injured livers was most pronounced at early time-points and slowly decreased over 8 weeks (Fig.1B). In contrast, the development of hepatic fibrosis, as quantified by Sirius red staining (Fig.1A) and hydroxyproline concentrations in liver tissue (Fig.1B), progressed almost linearly over time. The formation of blood vessels, as analyzed by immunofluorescent staining of $CD31^+$ endothelial cells, was strongly induced in progressive liver injury and largely paralleled the progression of fibrosis (Fig.1B). These observations demonstrated that angiogenesis and fibrosis progression closely correlate in experimental liver injury.

Functional *in vivo* µCT imaging allows accurate assessment of fibrosis-associated angiogenesis

In order to quantify hepatic blood vessels during fibrogenesis we established a contrast-enhanced µCT approach for *in vivo* imaging. To this end, we visualized the 3D micromorphology of hepatic blood vessels in animals treated repetitively with CCl_4 after 2, 4, 6, and 8 weeks and in healthy control animals from longitudinal µCT scan series, and we simultaneously quantified non-invasively the relative blood volume (rBV) in livers using an iodine-based contrast agent optimized for blood pool imaging [20]. Via 2D µCT images in transversal, sagittal and coronal planes as well as via 3D volume renderings, dual-energy flat-panel *in vivo* µCT enabled the non-invasive visualization of blood vessels in the liver with a spatial resolution of 35µm voxel side length (Fig.2A). Representative images and movies demonstrated that chronically injured livers showed a significantly higher amount of functional blood vessels as compared to vehicle-treated controls (Fig.2A, Suppl.Videos 1-2). In line, hepatic rBV values were significantly higher for animals challenged with CCl_4 for 6 weeks (25.7±0.9%) than for control animals (19.4±0.6%, $P<0.0005$) (Fig.2B), corroborating that fibrosis progression is paralleled by an increasing hepatic blood volume.

To assess the accuracy of *in vivo* µCT (which considers vessel functionality) vs. standard CD31-based immunohistochemistry (which does not consider vessel functionality), rBV values were correlated with the area fraction of $CD31^+$ endothelial cells (Fig.2C). Whereas hepatic rBV values determined by *in vivo* µCT ranged from 22.4±0.9% for animals exposed to CCl_4 for 2 weeks to 27.1±1.6% for animals challenged for 8 weeks (control animals: 19.4±0.6%), $CD31^+$ area fractions determined by *ex vivo* IHC ranged from 2.4±0.6% for injured livers after 2 weeks CCl_4 to 6.0±1.0% after 8 weeks of CCl_4 (control animals: 0.8±0.2%). A highly significant correlation between rBV values determined using *in vivo* µCT and *ex vivo* immunohistochemistry was observed ($R^2=0.9572$, $P<0.0001$, n=15), indicating that contrast-enhanced *in vivo* µCT is an accurate means for non-invasively assessing the hepatic blood volume during experimental fibrogenesis.

The spatial resolution of this *in vivo* µCT-based imaging technique, however, is limited to 35µm voxel side length, and newly formed blood vessels may partially be smaller. Therefore, we also perfused the animals with the lead-containing vascular casting agent Microfil and performed high-resolution *ex vivo* µCT scans. Whereas healthy livers showed a proper hierarchic vascular branching system, both for the central and portal vein system, high-resolution *ex vivo* µCT imaging of fibrotic livers revealed areas with sprouting

angiogenesis, in particular in the periphery of chronically injured livers (Fig.2D, Suppl.Videos 3-4).

In order to exclude model-specific effects related to toxic CCl_4-induced damage, we confirmed the close correlation between hepatic fibrosis and angiogenesis in a second mouse model of chronic liver injury (surgical bile duct ligation [BDL], resulting in progressive cholestatic liver injury). Twenty-one days after BDL or sham operation, mice were imaged using contrast-enhanced *in vivo* μCT, followed by Microfil perfusion and high-resolution *ex vivo* μCT imaging, and finally by histological validation. Livers from BDL-treated mice showed severe cholestatic damage with large necrotic areas, bridging fibrosis, leukocyte infiltration and neovascularization (Fig.3A). In line with the results obtained for CCl_4, using functional *in vivo* (Fig.3B, Suppl.Videos 5-6) and anatomical *ex vivo* (Fig.3C, Suppl.Videos 7-8) μCT imaging, a significant increase in the formation of new blood vessels was detected in livers with chronic cholestatic injury. Quantification of liver injury by serum ALT, of collagen deposition by hepatic hydroxyproline concentrations, and of $CD45^+$ leukocytes as well as $CD31^+$ endothelial cells by immunohistochemistry confirmed the presence of injury, inflammation, fibrosis and angiogenesis in BDL-induced liver damage (Fig.3D). Accordingly, rBV values were significantly higher in fibrotic (26.3±1.3%) vs. control livers (19.6±1.0%, $P<0.01$) (Fig.3D). Collectively, these findings from two independent experimental models for progressive liver fibrosis showed a strong association between liver fibrosis and angiogenesis, and they exemplify that functional *in vivo* and anatomical *ex vivo* μCT imaging can be used to monitor fibrosis-associated angiogenesis.

Distinct subsets of hepatic macrophages induce angiogenesis during fibrogenesis

Based on the pivotal role of monocytes and macrophages in the progression of liver inflammation and fibrosis [15], we hypothesized that hepatic macrophages could be the driving force for the formation of new blood vessels during fibrogenesis. Indeed, when mice were challenged repetitively with CCl_4 twice per week for up to 8 weeks, a continuous accumulation of $F4/80^+$ macrophages could be observed in injured livers (Fig.4A). Upon quantifying the F4/80 area fraction (three different sections per liver, n=15 mice), a massive increase of hepatic macrophages could be detected already at early stages of fibrosis after exposure to CCl_4 for 2 weeks (3.9±0.4% vs. 0.5±0.2% in healthy livers; $P<0.001$) (Fig.4B). The amount of infiltrated macrophages steadily increased upon prolonged exposure to CCl_4 (from 4.7±0.3% after 4 weeks to 6.9±0.8% after 8 weeks). In both models of progressive liver fibrosis, $F4/80^+$ macrophages were localized in close vicinity of newly formed and mainly periportally localized $CD31^+$ blood vessels in chronically injured livers (Fig.4C).

A further dissection of inflammatory macrophages (iMΦ) and Kupffer cells (KC) via FACS, based on their differential expression of F4/80 and CD11b, revealed a strong increase of $CD11b^+F4/80^+$ inflammatory monocyte-derived macrophages already very early in chronic liver injury, and iMΦ remained the predominant leukocyte population infiltrating throughout the progression of chronic liver diseases (Fig.4D).

To determine the pro-angiogenic activity of hepatic macrophage subsets during fibrogenesis, gene expression analyses of purely isolated iMΦ ($CD11b^+F4/80^+$), Kupffer cells (defined as $CD11b^{low}F4/80^{++}$ cells), primary hepatocytes, endothelial cells ($CD45^-CD146^+$) and hepatic

stellate cells ($CD45^-UV^+$) from injured and healthy control livers were performed after FACS-based cell sorting using quantitative real-time PCR. Although Kupffer cells and stellate cells were an important source of angiogenic factors in homeostasis (Fig.4E-F), only iMΦ showed a strongly increased expression of pro-angiogenic factors like VEGF-A (10.2-fold higher expression in injured vs. control livers) or MMP9 (3.5-fold higher expression in injured vs. control livers) upon liver injury. On the contrary, VEGF-A and MMP9 expression was strongly reduced in Kuppfer cells, hepatocytes, endothelial cells and hepatic stellate cells in CCl_4-treated livers (Fig.4E-F). Collectively, these findings strongly indicated that the distinct subset of monocyte-derived inflammatory macrophages actively promotes hepatic neovascularization during fibrogenesis.

Angiogenesis, but not fibrosis progression, is controlled by CCL2-dependent monocyte infiltration

Findings obtained both in mice and in humans demonstrated that the accumulation of inflammatory monocyte-derived macrophages in injured livers is critically controlled by the chemokine CCL2 (also termed monocyte chemoattractant protein-1, MCP-1)[15]. In order to provide functional evidence that infiltrating monocytes drive angiogenesis in liver fibrosis, we investigated the effect of specific pharmacological inhibition of CCL2 on fibrosis-associated angiogenesis by using the ‘Spiegelmer’ mNOX-E36 [12]. In fact, administration of mNOX-E36 during CCl_4-induced chronic liver injury significantly reduced infiltrating leukocytes, particularly macrophages (as evidenced by F4/80 immunohistochemistry, Fig.5A). In line with prior observations [12], mNOX-E36 treatment did neither significantly diminish fibrosis progression nor ALT or AST serum activity in CCl_4 injured livers (Fig.5A, Suppl. Fig.1). However, blood vessel formation was significantly reduced in mNOX-E36 treated animals (Fig.5A+B), and immunofluorescence co-stainings revealed a simultaneous reduction of $F4/80^+$ liver macrophages and $CD31^+$ blood vessels over 2-8 weeks of CCl_4 injury in case of mNOX-E36 administration (Fig.5A). Importantly, administration of the CCL2 inhibitor mNOX-E36 specifically reduced the amount of $CD11b^+F4/80^+$ iMΦ as assessed by FACS analysis from intrahepatic leukocytes (Fig.5C), in line with prior findings from our group [12].

In order to confirm and to non-invasively monitor anti-angiogenic therapy effects of mNOX-E36 in mice suffering from CCl_4-induced liver fibrosis under *in vivo* hepatic blood flow conditions, functional μCT imaging was performed. Contrast-enhanced *in vivo* μCT scans demonstrated a significant reduction of fibrosis-associated hepatic blood vessels as a therapeutic effect of mNOX-E36 treatment (Fig.5D, Suppl.Video 9). Whereas rBV values rose continuously during the course of CCl_4 administration (+15.5%, +20.1%, +32.5% and +39.7% after 2, 4, 6, 8 weeks, respectively; $P<0.01$) as compared to control animals, the CCl_4-induced increase in rBV was almost completely blocked by mNOX-E36 treatment (Fig.5E). At each time-point evaluated, rBV values in the mNOX-E36 therapy group were significantly lower than those in the untreated CCl_4-group (−18.8%, −19.4%, −25.9% and −24.4% after 2, 4, 6, 8 weeks, respectively; $P<0.05$). Importantly, the effect of CCL2 inhibition was specific to injured livers, because no differences in splenic rBV values were observed in the corresponding animals (Fig.5E). Gene expression profiling of livers from mice treated with CCl_4 and CCl_4+mNOX-E36 for 6 weeks revealed that the reduced

numbers of macrophages were reflected by lower expression of macrophage-associated genes such as cytokines, M1/2 proliferation markers and pro-angiogenic factors (Suppl.Fig. 1).

In order to exclude that CCL2 or mNOX-E36 itself had direct effects on blood vessel formation, two *in vitro* experiments were performed. Firstly, primary endothelial cells were isolated from livers of healthy mice, cultured in VEGF-containing medium with or without the presence of mNOX-E36, and either stimulated with CCL2 or left unstimulated (Suppl.Fig.2A-B). Secondly, using similar culture conditions, an angiogenic sprouting assay with dissected 0.5mm-thin aortic rings of c57bl/6 wild type mice was performed, analysing the number of sprouts after 10 days (Suppl. Fig.2C-D). Importantly, in both cases of CCL2-stimulation or unstimulated controls, mNOX-E36 treatment did neither affect proliferation and viability of the hepatic endothelium, nor the sprouting of aortic rings (Suppl.Fig.2). Taken together, our results demonstrate that the pharmacological inhibition of the chemokine CCL2 effectively blocks fibrosis-associated angiogenesis in chronically injured livers by inhibiting infiltrating CCL2-dependent monocytes.

Macrophage-dependent angiogenesis during chronic liver injury is primarily important for portal vein sprouting

In comparison to functional *in vivo* μCT, which spatial resolution ends at ~35μm, anatomical high-resolution *ex vivo* μCT imaging, allowing a spatial resolution of ~12μm, indicated an even stronger anti-angiogenic effect of CCL2 inhibition, especially in the periphery of mNOX-E36 treated livers (Fig.6A, Suppl.Video 10). After semi-automatic vessel tree segmentation of the central and portal vein system, the total number of branching points as well as the number of branching points per rising branching order were quantified (Fig.6B). Whereas CCl_4-induced toxic liver injury caused a significant increase in branching points in both the central (+59.5%) and portal (+64.0%) vein system, the CCL2-dependent inhibition of macrophage migration resulted in a clear reduction of newly formed vessels, primarily those associated with the portal vein; as compared to the CCl_4 group, 17.6% less branching points of the central vein, and 29.5% less branching points of the portal vein were detected upon CCL2-inhibition ($P<0.05$ for both; Fig.6C). Comparing the distribution of branching points per rising branching order in both tracts, healthy livers demonstrated an almost equal distribution of branching points from the 1^{st} to the 9^{th} order (Fig.6D). In progressing liver fibrosis (6 weeks of repetitive CCl_4 injections), the formation of new hepatic blood vessels was morphologically linked to a strong increase of branching points in the periphery of both the central and the portal vein: the relative number of 9^{th} order branching points increased significantly (5.6-fold, $P<0.0001$), and moreover, 10^{th} and 11^{th} order branching points were newly generated. Conversely, in livers exposed to CCl_4 and treated with mNOX-E36, the number of 9^{th} order branching points was again reduced, and this effect was much more prominent in the portal vein (-52.8%) than in the central vein (-25.5%) ($P<0.0001$; Fig.6D). These findings were confirmed using the BDL model (Suppl.Fig.3). Collectively, these highly detailed 3D micromorphological analyses demonstrated that the macrophage-dependent angiogenesis during chronic liver injury is largely confined to portal veins and that pharmacological inhibition of CCL2-mediated

inflammatory monocyte infiltration primarily reduces angiogenic vessel sprouting in the portal vein system.

Differential impact of fibrosis and angiogenesis on portal hypertension

In order to further investigate the association between fibrosis progression, portal vein-related vessel sprouting and portal hypertension, we used contrast-enhanced μCT to quantify the portal vein diameter, as a measure of portal hypertension [21, 22, 23], 3-4 transversal slices above the junction of the superior mesenteric and splenic vein (Fig.7A). Interestingly, portal vein diameter increased significantly during progression of liver fibrosis (e.g. 1.68±0.07 mm for animals challenged with CCl_4 for 6 weeks vs. 1.13±0.06 mm for control animals), but were not significantly influenced by mNOX-E36 treatment (e.g., 1.69±0.05 mm for animals treated with CCl_4 & mNOX-E36 for 6 weeks; Fig.7B). In detail, a highly significant correlation between portal vein diameters determined using *in vivo* μCT and *ex vivo* quantified hydroxyproline content was observed (R^2=0.8194, P<0.001, n=30; Fig.7C). In contrast, no significant correlation was found between portal vein diameters and *in vivo* quantified rBVs (R^2=0.3795, P=0.0579, n=30; Fig.7D). These findings strongly indicate that portal hypertension may be more directly caused by the progressive fibrosis itself (extracellular deposition of collagens causing increased liver stiffness) than by pathological fibrosis-associated angiogenesis (sprouting blood vessels causing additional micro-shunts).

Discussion

Chronic hepatic inflammation is regarded as a key requirement for the progression of liver fibrosis, but its role in promoting fibrosis-associated angiogenesis has not yet been elucidated. Moreover, although angiogenesis is commonly observed in patients with hepatic cirrhosis [2], the functional implications of pathological angiogenesis in progressive liver disease have remained largely obscure. Inflammation-associated angiogenesis might contribute not only to the initiation of liver fibrosis, but also in the progression from fibrosis into cirrhosis, and from cirrhosis into hepatocellular carcinoma (HCC) [6, 7, 9]. Thus far, however, studies on the role of angiogenesis in progressive liver disease have been largely restricted to immunohistochemical endpoint analyses. We have here established and employed *in vivo* and *ex vivo* μCT-based imaging techniques, alongside conventional molecular methodologies, to demonstrate that I) even at the initial stages of liver fibrosis, angiogenesis is induced; II) fibrosis stage correlates with extent of hepatic neovascularization; III) infiltrating bone marrow-derived inflammatory monocytes mediate fibrosis-associated angiogenesis induction; IV) the pharmacological inhibition of CCL2 attenuates monocyte infiltration and angiogenesis, but not fibrosis progression; V) these effects are primarily attributable to changes in the portal vein system; and VI) portal hypertension is rather driven by extracellular collagen deposition than by fibrosis-associated pathological angiogenesis.

Prior studies have indicated that hypoxia increases the expression of the prototypic pro-angiogenic factor VEGF, thereby promoting angiogenesis and potentially also the progression from fibrosis to cirrhosis and to HCC [1, 3, 7]. VEGF enhances endothelial cell proliferation, promotes vessel sprouting and branching, and increases microvessel

permeability [24]. Besides classical hypoxia-induced and HIF1-mediated VEGF expression, also inflammatory cells might elevate the levels of pro-angiogenic factors in injured livers [10, 25]. In experimental models of cancer progression, infiltrating inflammatory macrophages are a major mediator of tumor angiogenesis [26]. In line, inflammatory cells migrating into injured livers have been implicated in HCC-associated angiogenesis [8, 9]. Detailed analyses on the molecular link between inflammatory monocyte infiltration, angiogenesis and liver fibrosis progression, however, have not yet been performed to date, which can be at least partially explained by the relative lack of suitable imaging techniques to non-invasively, longitudinally and quantitatively monitor angiogenesis.

The chemokine-dependent accumulation of monocyte-derived macrophages has been identified as an important mechanism for perpetuating hepatic inflammation and promoting fibrogenesis in experimental mouse models as well as in human liver diseases [15]. Upon experimental organ injury in mice, the chemokine receptor CCR2 and its ligand CCL2 (MCP-1) promote monocyte subset accumulation in the liver, in particular of Ly6C+ (Gr1+) monocytes. These monocyte-derived macrophages release pro-inflammatory cytokines and can directly activate pro-fibrogenic hepatic stellate cells, the main collagen-producing cells in the liver [15]. Our study significantly extends these previous findings, by demonstrating that infiltrating CCL2-dependent inflammatory monocytes also provide pro-angiogenic signals, likely via the production and release of VEGF-A and other factors like MMP9.

To test our hypothesis that these infiltrating monocytes are essential in mediating fibrosis-associated angiogenesis, the CCL2/CCR2-dependent migration of inflammatory monocytes into injured livers was inhibited using a novel CCL2 inhibitor, the ‘Spiegelmer’ mNOX-E36 [12]. Findings from quantitative *in vivo* and *ex vivo* μCT imaging of functional liver blood vessels, coupled to FACS and gene expression analyses, revealed that the inhibition of CCL2-dependent inflammatory monocytes by mNOX-E36 significantly reduced the formation of new blood vessels in progressive liver fibrosis. Thus, mNOX-E36, whose human equivalent is currently being evaluated in a phase II clinical trial for the treatment of diabetic nephropathy (www.clinicaltrials.gov, NCT01547897), appears to be an attractive therapeutic approach for reducing the inflammation-associated angiogenesis in progressive liver fibrosis. Strikingly, the inhibition of CCL2-dependent monocyte infiltration did not affect liver fibrosis progression *per se*, in line with prior work from our group [12]. This further demonstrates that the inhibition of macrophage-mediated angiogenesis induction did not attenuate the progression from early-to-late stage liver fibrosis, indicating that initially angiogenesis is a consequence of inflammation, rather than a cause for disease progression. However, at later stages, the contribution of pathological angiogenesis to chronic liver disorders is anticipated to become more and more causal, in particular during the transition from cirrhosis to HCC, and the subsequent progression and spread of HCC.

Besides identifying a yet unrecognized cellular and molecular mechanism of fibrosis-associated angiogenesis, our study may also be of interest for developing future imaging strategies in the management of patients with chronic liver disease. The current ‘gold standard’ of fibrosis assessment is needle biopsy of the liver, carrying the risk of bleeding complications as well as sampling errors [27]. In the last couple of years, only few ultrasound and magnetic resonance (MR) based methods have been evaluated for non-

invasively measuring liver stiffness [4, 28, 29]. Some studies reported on the non-invasive quantification of the portal vein diameter via MR or ultrasound as a measure of portal hypertension [21, 22, 23]. In addition, very few studies described molecular imaging approaches for the *in vivo* assessment of liver fibrosis via collagen or elastin specific contrast agents in experimental settings [30, 31]. However, due to the fact that no anti-fibrotic drugs have been approved up to date [4], only limited data exist for these imaging approaches for therapy monitoring. In contrast, functional imaging approaches like quantitative contrast-enhanced CT enable the visualization of liver blood vessels, the non-invasive quantification of the hepatic rBV, which correlates significantly with the amount of newly formed blood vessels during fibrosis progression, and the quantification of the portal vein diameter, which correlates with degree of portal hypertension. With respect to pathophysiological circulation conditions in fibrotic livers, µCT imaging can assess microstructural and functional changes in the hepatic vascular network and provides in addition the unique opportunity to monitor anti-angiogenic therapy effects. We here show that µCT imaging is highly useful for quantitatively assessing fibrosis-associated angiogenesis, and for monitoring anti-inflammatory and anti-angiogenic therapy effects in progressive liver disease, indicating that anatomical and functional contrast-enhanced CT imaging might hold great potential for facilitating the bench-to-bedside translation of novel targeted treatments and therapeutic interventions.

Supplementary Methods

Liver enzymes, histology, immunohistochemistry, and fluorescence microscopy

Liver injury and fibrosis were determined by alanine aminotransferase (ALT) or aspartate transaminase (AST) activity, histology (hematoxylin and eosin, Sirius red stainings) and biochemical methods (hydroxyproline content), as described earlier [1]. Immunohistochemical stainings of liver sections for CD45 and F4/80 were counted by a blinded pathologist, as published earlier [2]. Immunofluorescent stainings were performed using frozen sections and a rat anti-mouse CD31 antibody (BD Biosciences, San José, CA, USA) for blood vessel staining and a rat anti-mouse F4/80 antibody (AbD Serotec, Oxford, UK) for the assessment of macrophages. Secondary antibodies (donkey anti-rat Alexa Fluor 488 and donkey anti-rat Cy3) were obtained from Dianova (Hamburg, Germany). Hoechst 33258 (Sigma Aldrich, Taufkirchen, Germany) was used for nuclei counterstaining, and sections were mounted using Mowiol. Fluorescence microscopy was performed using an Axio Imager M2 microscope (Carl Zeiss Microimaging GmbH, Göttingen, Germany) and a high-resolution camera (AxioCam MRm Rev.3, Carl Zeiss Microimaging GmbH, Göttingen, Germany). For quantifying the formation of blood vessels in livers, 3 micrographs from 3 representative sections per liver and from 3 different livers per model and condition were analyzed for each condition. Area fractions of CD31-positive blood vessels and of F4/80-positive macrophages were determined. Quantifications of blood vessel density and macrophages were performed using the AxioVision Rel 4.8 software (Zeiss, Göttingen, Germany).

Isolation and flow cytometric analysis of blood and intrahepatic leukocytes

Blood was gained from the right ventricle, lysed with Pharm Lyse (BD Biosciences, San José, CA, USA), and was washed with Hank's buffered salt solution (HBSS) containing 5 μm EDTA and 0.5% BSA before FACS analysis. Hepatic leukocytes were isolated and multi-color flow cytometric analyses were done as described before [2]. Murine macrophages were isolated from minced and collagenase-treated livers by magnetic bead separation using a biotinylated anti-F4/80 antibody and streptavidin-magnetic beads (Miltenyi Biotech, Bergisch-Gladbach, Germany) [1].

Real-time gene expression analysis

After harvesting, livers were snap-frozen in liquid nitrogen and RNA was purified by pegGOLD (peqLab, Erlangen, Germany). RNA from sorted cells was isolated using the ArrayPure Nano-Scale RNA Purification Kit (Epicentre, Singapore, Singapore). cDNA was generated using a cDNA synthesis kit (Roche, Basel, Switzerland), and quantitative real-time PCR (qPCR) analyses were performed using SYBR Green Reagent (Invitrogen, Carlsbad, CA, USA). Primer sequences are available upon request.

Liver cell isolation and endothelial cell viability assay

To isolate hepatic liver cells, mice were anaesthetized using 7 mg/kg body weight Xylazine and 105 mg/kg body weight of Ketamine. Primary murine hepatocytes were isolated via perfusion of the liver with collagenase type 2 and a type 2-S trypsin inhibitor from *Glycine max* (soybean) (Sigma-Aldrich, St. Louis, MO, USA), followed by gentle dissection of the liver. Primary hepatic stellate cells were isolated from livers of 8 weeks old C57BL/6 mice via their UV signal and by excluding endothelial cells (expressing CD31) and leukocytes ($CD45^+$) [3]. Primary murine endothelial cells were isolated by FACS sorting (Aria II, BD) based on positive staining for CD31 and negative staining for CD45 (excluding leukocytes) as well as in the UV-channel (excluding stellate cells). Liver endothelial cells were cultured with an endothelial cell growth medium that contained VEGF (ScienCell, Carlsbad, CA, USA) on collagen I-coated tissue culture treated polystyrene in a humidified incubator at 37°C with 5% CO2. After 16h, medium containing non-adherent cells was replaced completely, and cells were either left untreated or were stimulated for another 24h with murine recombinant CCL2 (100 ng/mL) (PeproTech Inc., New Jersey, USA), mNOX-E36 (200μg/mL), or CCL2 + mNOX-E36. To analyze the proliferation and viability of the cells, a 3-(4,5-dimethylthiazol-2-yl)-2,5-diphenyltetrazolium bromide (MTT) assay was performed according to manufacturer's protocol.

Aortic sprouting assay

Thoracic aortae were dissected from c57BL/6 wildtype mice, washed three times with PBS, cut into 0.5 mm thin rings and embedded in Matrigel 356231 (BD Biosciences, San Jose, CA, USA), as described before [4]. Once embedded, rings were cultured on 24-well plates in endothelial cell growth medium that contained VEGF (ScienCell, Carlsbad, CA, USA). Additionally, rings were continuously stimulated with murine recombinant CCL2 (100 ng/mL), mNOX-E36 (200μg/mL), CCL2 + mNOX-E36, or were left untreated (n=3 aortic rings per condition). Medium was replaced every second day. 10 days after embedding, at the end

of the exponential growth phase, phase-contrast microscopy of the rings was performed using an EVOS® FL cell imaging system (Life Technologies, Carlsbad, CA, USA) and primary sprouts per ring were counted. Images from different focusing planes were taken and stacked using CombineZM image stacking software (http://www.hadleyweb.pwp.blueyonder.co.uk/index.htm).

Statistical analysis

All data are presented as mean ± standard deviation. For assessing statistical significance, the two-tailed unpaired Student's t-test and Pearson's correlation were used. P values <0.05 were considered as statistically significant, and P values of <0.01 were considered as highly significant. All statistical analyses were performed using GraphPadPrism 5.0 (San Diego, CA, USA).

Supplementary Material

Refer to Web version on PubMed Central for supplementary material.

Acknowledgments

The authors thank Aline Roggenkamp, Carmen Tag and Sibille Sauer-Lehnen for excellent technical assistance and NOXXON Pharma AG (Berlin, Germany) for providing mNOX-E36.

Funding: This work was supported by German Research Foundation (DFG; SFB/TRR57, TA434/2-1, EH412/1-1 and LA2937/1-2), Interdisciplinary Center for Clinical Research (IZKF Aachen) and European Research Council (ERC-StG-309495-NeoNaNo).

References

1. Corpechot C, Barbu V, Wendum D, Kinnman N, Rey C, Poupon R, et al. Hypoxia-induced VEGF and collagen I expressions are associated with angiogenesis and fibrogenesis in experimental cirrhosis. Hepatology. 2002; 35:1010–21. [PubMed: 11981751]
2. Medina J, Arroyo AG, Sanchez-Madrid F, Moreno-Otero R. Angiogenesis in chronic inflammatory liver disease. Hepatology. 2004; 39:1185–95. [PubMed: 15122744]
3. Tugues S, Fernandez-Varo G, Munoz-Luque J, Ros J, Arroyo V, Rodes J, et al. Antiangiogenic treatment with sunitinib ameliorates inflammatory infiltrate, fibrosis, and portal pressure in cirrhotic rats. Hepatology. 2007; 46:1919–26. [PubMed: 17935226]
4. Schuppan D, Kim YO. Evolving therapies for liver fibrosis. J Clin Invest. 2013; 123:1887–901. [PubMed: 23635787]
5. Hong F, Chou H, Fiel MI, Friedman SL. Antifibrotic activity of sorafenib in experimental hepatic fibrosis: refinement of inhibitory targets, dosing, and window of efficacy in vivo. Dig Dis Sci. 2013; 58:257–64. [PubMed: 22918681]
6. Coulon S, Heindryckx F, Geerts A, Van Steenkiste C, Colle I, Van Vlierberghe H. Angiogenesis in chronic liver disease and its complications. Liver Int. 2011; 31:146–62. [PubMed: 21073649]
7. Rosmorduc O, Housset C. Hypoxia: a link between fibrogenesis, angiogenesis, and carcinogenesis in liver disease. Semin Liver Dis. 2010; 30:258–70. [PubMed: 20665378]
8. Capece D, Fischietti M, Verzella D, Gaggiano A, Cicciarelli G, Tessitore A, et al. The inflammatory microenvironment in hepatocellular carcinoma: a pivotal role for tumor-associated macrophages. Biomed Res Int. 2013; 2013:187204. [PubMed: 23533994]
9. Matsubara T, Kanto T, Kuroda S, Yoshio S, Higashitani K, Kakita N, et al. TIE2-expressing monocytes as a diagnostic marker for hepatocellular carcinoma correlates with angiogenesis. Hepatology. 2013; 57:1416–25. [PubMed: 22815256]

Europe PMC Funders Author Manuscripts

10. Coulon S, Legry V, Heindryckx F, Van Steenkiste C, Casteleyn C, Olievier K, et al. Role of vascular endothelial growth factor in the pathophysiology of nonalcoholic steatohepatitis in two rodent models. Hepatology. 2013; 57:1793–805. [PubMed: 23299577]
11. De Palma M, Lewis CE. Macrophage regulation of tumor responses to anticancer therapies. Cancer cell. 2013; 23:277–86. [PubMed: 23518347]
12. Baeck C, Wehr A, Karlmark KR, Heymann F, Vucur M, Gassler N, et al. Pharmacological inhibition of the chemokine CCL2 (MCP-1) diminishes liver macrophage infiltration and steatohepatitis in chronic hepatic injury. Gut. 2012; 61:416–26. [PubMed: 21813474]
13. Karlmark KR, Weiskirchen R, Zimmermann HW, Gassler N, Ginhoux F, Weber C, et al. Hepatic recruitment of the inflammatory Gr1+ monocyte subset upon liver injury promotes hepatic fibrosis. Hepatology. 2009; 50:261–74. [PubMed: 19554540]
14. Ramachandran P, Pellicoro A, Vernon MA, Boulter L, Aucott RL, Ali A, et al. Differential Ly-6C expression identifies the recruited macrophage phenotype, which orchestrates the regression of murine liver fibrosis. Proceedings of the National Academy of Sciences of the United States of America. 2012; 109:E3186–95. [PubMed: 23100531]
15. Tacke F. Functional role of intrahepatic monocyte subsets for the progression of liver inflammation and liver fibrosis in vivo. Fibrogenesis Tissue Repair. 2012; 5(Suppl 1):S27. [PubMed: 23259611]
16. Ehling J, Lammers T, Kiessling F. Non-invasive imaging for studying anti-angiogenic therapy effects. Thromb Haemost. 2013; 109:375–90. [PubMed: 23407722]
17. Karlmark KR, Zimmermann HW, Roderburg C, Gassler N, Wasmuth HE, Luedde T, et al. The fractalkine receptor CX(3)CR1 protects against liver fibrosis by controlling differentiation and survival of infiltrating hepatic monocytes. Hepatology. 2010; 52:1769–82. [PubMed: 21038415]
18. Hammerich L, Bangen JM, Govaere O, Zimmermann HW, Gassler N, Huss S, et al. Chemokine receptor CCR6-dependent accumulation of gammadelta T cells in injured liver restricts hepatic inflammation and fibrosis. Hepatology. 2014; 59:630–642. [PubMed: 23959575]
19. Gremse F, Grouls C, Palmowski M, Lammers T, de Vries A, Grull H, et al. Virtual elastic sphere processing enables reproducible quantification of vessel stenosis at CT and MR angiography. Radiology. 2011; 260:709–17. [PubMed: 21788527]
20. Ehling J, Theek B, Gremse F, Baetke S, Mockel D, Maynard J, et al. Micro-CT Imaging of Tumor Angiogenesis: Quantitative Measures Describing Micromorphology and Vascularization. The American journal of pathology. 2014; 184:431–441. [PubMed: 24262753]
21. Zhang J, Tao R, You Z, Dai Y, Fan Y, Cui J, et al. Gamna-Gandy bodies of the spleen detected with susceptibility weighted imaging: maybe a new potential non-invasive marker of esophageal varices. PloS one. 2013; 8:e55626. [PubMed: 23383250]
22. Lessa AS, Paredes BD, Dias JV, Carvalho AB, Quintanilha LF, Takiya CM, et al. Ultrasound imaging in an experimental model of fatty liver disease and cirrhosis in rats. BMC veterinary research. 2010; 6:6. [PubMed: 20113491]
23. O'Donohue J, Ng C, Catnach S, Farrant P, Williams R. Diagnostic value of Doppler assessment of the hepatic and portal vessels and ultrasound of the spleen in liver disease. European journal of gastroenterology and hepatology. 2004; 16:147–55. [PubMed: 15075987]
24. Carmeliet P, Jain RK. Molecular mechanisms and clinical applications of angiogenesis. Nature. 2011; 473:298–307. [PubMed: 21593862]
25. Avraham-Davidi I, Yona S, Grunewald M, Landsman L, Cochain C, Silvestre JS, et al. On-site education of VEGF-recruited monocytes improves their performance as angiogenic and arteriogenic accessory cells. The Journal of experimental medicine. 2013; 210:2611–25. [PubMed: 24166715]
26. Solinas G, Germano G, Mantovani A, Allavena P. Tumor-associated macrophages (TAM) as major players of the cancer-related inflammation. J Leukoc Biol. 2009; 86:1065–73. [PubMed: 19741157]
27. Bedossa P, Dargere D, Paradis V. Sampling variability of liver fibrosis in chronic hepatitis C. Hepatology. 2003; 38:1449–57. [PubMed: 14647056]
28. Castera L. Noninvasive methods to assess liver disease in patients with hepatitis B or C. Gastroenterology. 2012; 142:1293–302 e4. [PubMed: 22537436]

29. Huwart L, Sempoux C, Vicaut E, Salameh N, Annet L, Danse E, et al. Magnetic resonance elastography for the noninvasive staging of liver fibrosis. Gastroenterology. 2008; 135:32–40. [PubMed: 18471441]

30. Ehling J, Bartneck M, Fech V, Butzbach B, Cesati R, Botnar R, et al. Elastin-based molecular MRI of liver fibrosis. Hepatology. 2013; 58:1517–8. [PubMed: 23424008]

31. Polasek M, Fuchs BC, Uppal R, Schuhle DT, Alford JK, Loving GS, et al. Molecular MR imaging of liver fibrosis: a feasibility study using rat and mouse models. J Hepatol. 2012; 57:549–55. [PubMed: 22634342]

References for Supplementary Methods

1. Bartneck M, Ritz T, Keul HA, Wambach M, Bornemann J, Gbureck U, et al. Peptide-functionalized gold nanorods increase liver injury in hepatitis. ACS Nano. 2012; 6:8767–77. [PubMed: 22994679]

2. Heymann F, Hammerich L, Storch D, Bartneck M, Huss S, Russeler V, et al. Hepatic macrophage migration and differentiation critical for liver fibrosis is mediated by the chemokine receptor C-C motif chemokine receptor 8 in mice. Hepatology. 2012; 55:898–909. [PubMed: 22031018]

3. Hammerich L, Bangen JM, Govaere O, Zimmermann HW, Gassler N, Huss S, et al. Chemokine receptor CCR6-dependent accumulation of gammadelta T cells in injured liver restricts hepatic inflammation and fibrosis. Hepatology. 2014; 59:630–642. [PubMed: 23959575]

4. Baker M, Robinson SD, Lechertier T, Barber PR, Tavora B, D'Amico G, et al. Use of the mouse aortic ring assay to study angiogenesis. Nature protocols. 2011; 7:89–104.

Europe PMC Funders Author Manuscripts

Europe PMC Funders Author Manuscripts

Summary box: Significance of this study

What is already known about this subject?

- Although millions of people worldwide suffer from liver fibrosis and cirrhosis, non-invasive imaging techniques for quantitatively monitoring the progression of liver fibrosis and potential therapy effects in preclinical or clinical settings are currently limited.
- In advanced liver fibrosis, angiogenesis has been observed in human patients as well as in experimental animal models for chronic hepatic injury.
- Although fibrosis-associated angiogenesis is regarded as a promoting factor for the transition from chronic injury to hepatocellular carcinoma, the mechanisms of fibrosis-associated angiogenesis remain largely obscure.

What are the new findings?

- An innovative non-invasive contrast-enhanced functional *in vivo* micro-CT approach was established in experimental liver injury models in mice and validated by histological and anatomical *ex vivo* micro-CT based microstructural analyses.
- By using these innovative imaging techniques, we demonstrate that I) even at the initial stages of liver fibrosis, angiogenesis is induced; II) fibrosis stage correlates with extent of hepatic neovascularization; III) infiltrating bone marrow-derived inflammatory monocytes mediate fibrosis-associated angiogenesis induction; IV) pharmacological inhibition of CCL2 attenuates monocyte infiltration and angiogenesis, but not fibrosis progression; V) these effects are primarily attributable to changes in the portal vein system; and VI) portal hypertension is rather driven by extracellular collagen deposition than by fibrosis-associated pathological angiogenesis.

How might it impact on clinical practice in the foreseeable future?

- The establishment of a novel non-invasive imaging technique for monitoring fibrosis-associated angiogenesis in the liver and the identification of CCL2-dependent infiltrating monocytes as the driving force of inflammation-associated hepatic blood vessel expansion during fibrosis progression may advance diagnostics and allow novel therapeutic approaches in chronic liver diseases.

Europe PMC Funders Author Manuscripts

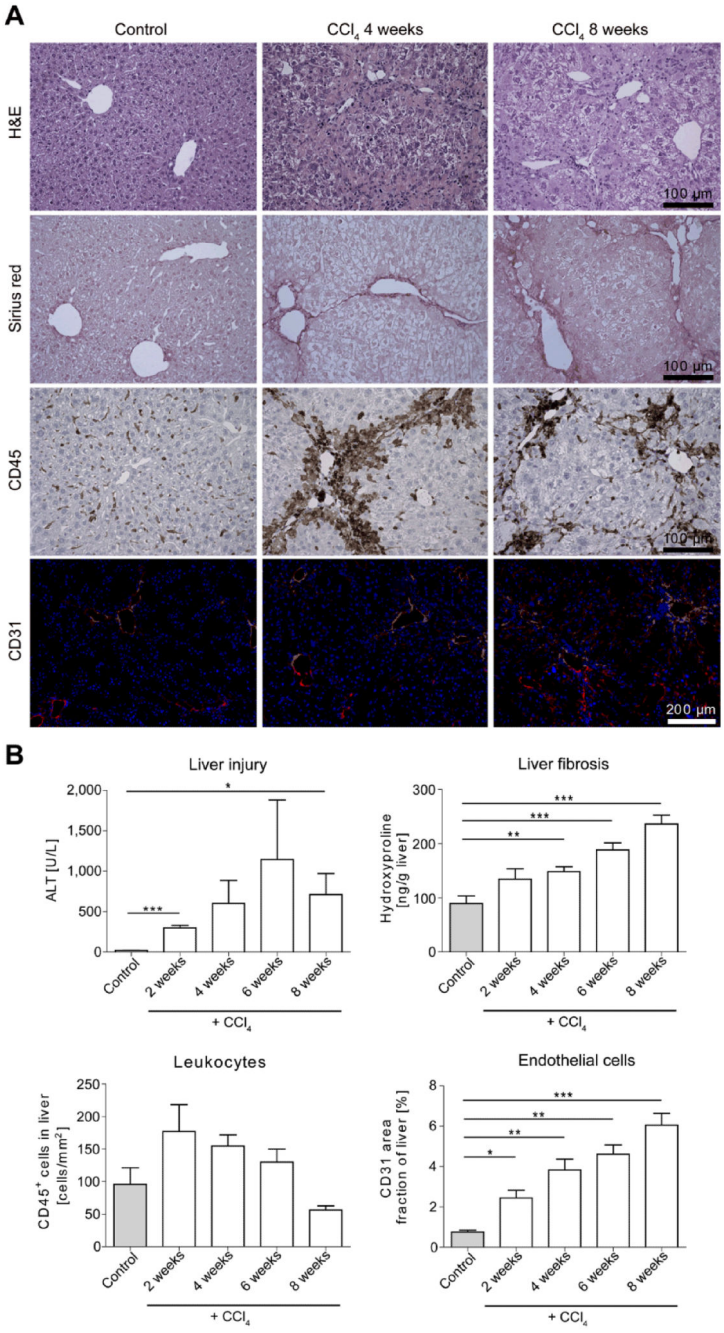

Figure 1. Association among chronic liver injury, inflammation, hepatic fibrosis and angiogenesis

(A) Chronic toxic liver injury was induced by repetitive i.p. injections of CCl_4 in c57BL/6 mice, and mice were sacrificed 48 hours after the last injection of CCl_4. Control mice received corn oil for 6 weeks. Representative H&E staining, Sirius red (fibrotic fibers in red), CD45 immunohistochemistry (leukocytes), and CD31 immunofluorescence (blood vessels) of controls and after 4 or 8 weeks CCl_4. (B) Serum ALT activity (liver injury), hepatic hydroxyproline content (collagen deposition), $CD45^+$ cells in liver sections (hepatic inflammation), and area fraction of $CD31^+$ endothelial cells (quantification of

neovascularisation). Data are shown as mean±SD (n=15 mice). ***P<0.001, **P<0.01 and *P<0.05 (Student's t test).

Europe PMC Funders Author Manuscripts

Europe PMC Funders Author Manuscripts

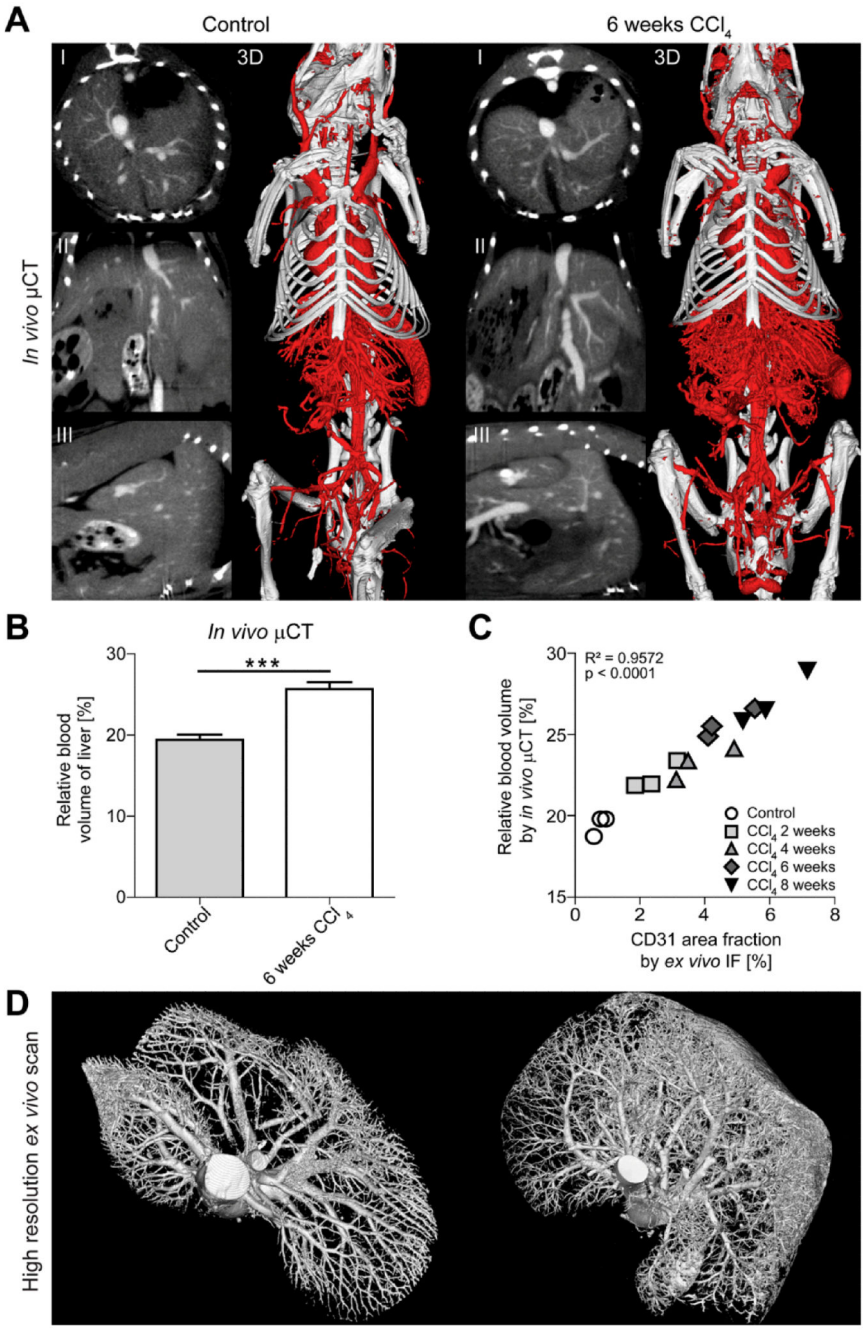

Figure 2. Functional and anatomical µCT imaging of angiogenesis in CCl_4-induced liver fibrosis

(A) Visualization of hepatic blood vessels by *in vivo* µCT using an iodine-based blood pool contrast agent (eXIA 160XL), resulting in a spatial resolution of 35µm voxel side length (2D cross-sectional images in transversal (I), sagittal (II) and coronal (III) planes, as well as representative pictures of 3D volume renderings). (B) Non-invasive µCT-based quantification of the relative blood volume (rBV) in fibrotic and healthy livers. (C) A highly significant correlation was found between hepatic rBV determined using *in vivo* µCT and area fraction of CD31 determined using *ex vivo* immunofluorescence (IF) staining. Data are

shown as mean±SD; n=15 mice; ***P<0.001 (Student's t test). Correlation analyses were performed by calculating R^2 (square of *Pearson* correlation coefficient). (D) High-resolution *ex vivo* μCT imaging (after perfusion with Microfil, a lead-containing radiopaque contrast agent) enables a detailed 3D examination of vascular microarchitecture of healthy liver (left) and after 6 weeks CCl_4 (right). Spatial resolution: 12μm voxel side length.

Europe PMC Funders Author Manuscripts

Europe PMC Funders Author Manuscripts

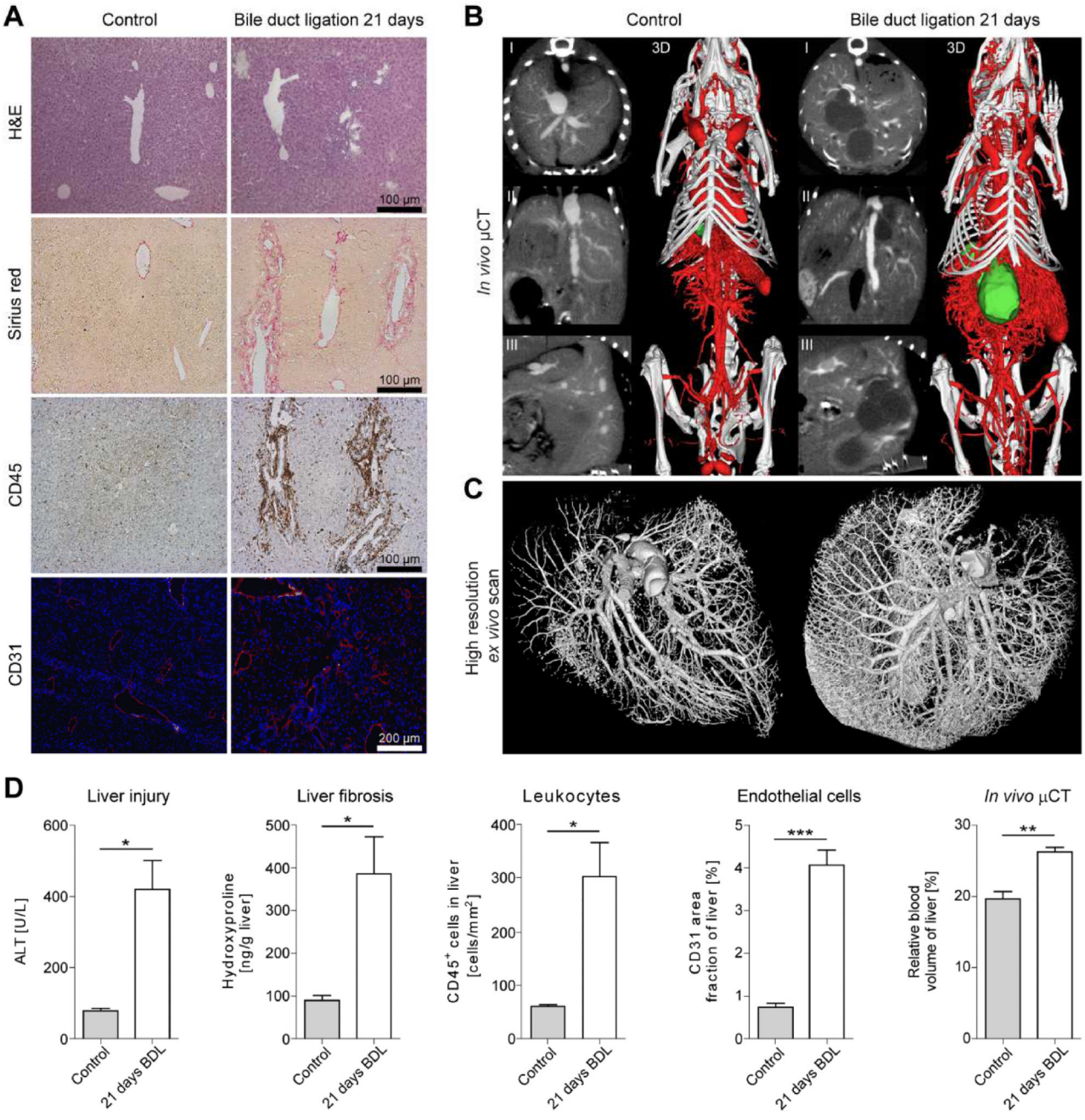

Figure 3. Association between fibrosis and angiogenesis in bile duct ligation-induced cholestatic liver injury

Chronic cholestatic liver injury was induced by surgical bile duct ligation (BDL) in c57BL/6 mice. Control animals received sham operations. Mice were imaged and sacrificed 21 days after surgery. (A) H&E staining, Sirius red staining (fibrosis), CD45 immunohistochemistry (inflammation) and CD31 immunofluorescence (blood vessel formation). *(B-C)* Functional *in vivo* (B) and morphological high-resolution *ex vivo* µCT imaging (C) of liver blood vessels from control and from BDL-treated mice (I: transversal, II: sagittal, III: coronal 2D cross-sectional images). Segmented gall bladders (green) illustrate gall bladder hydrops and

cholestasis after BDL. (D) Quantification of liver injury via ALT activity in serum, of liver fibrosis by hepatic hydroxyproline levels, of hepatic inflammation by quantifying $CD45^+$ cells, of hepatic blood vessels by determining the CD31 area fraction, and of the hepatic rBV, determined non-invasively using contrast-enhanced *in vivo* μCT. Results are shown as mean±SD (n=8 mice). ***$P<0.001$, **$P<0.01$ and *$P<0.05$ (Student's *t* test).

Europe PMC Funders Author Manuscripts

Europe PMC Funders Author Manuscripts

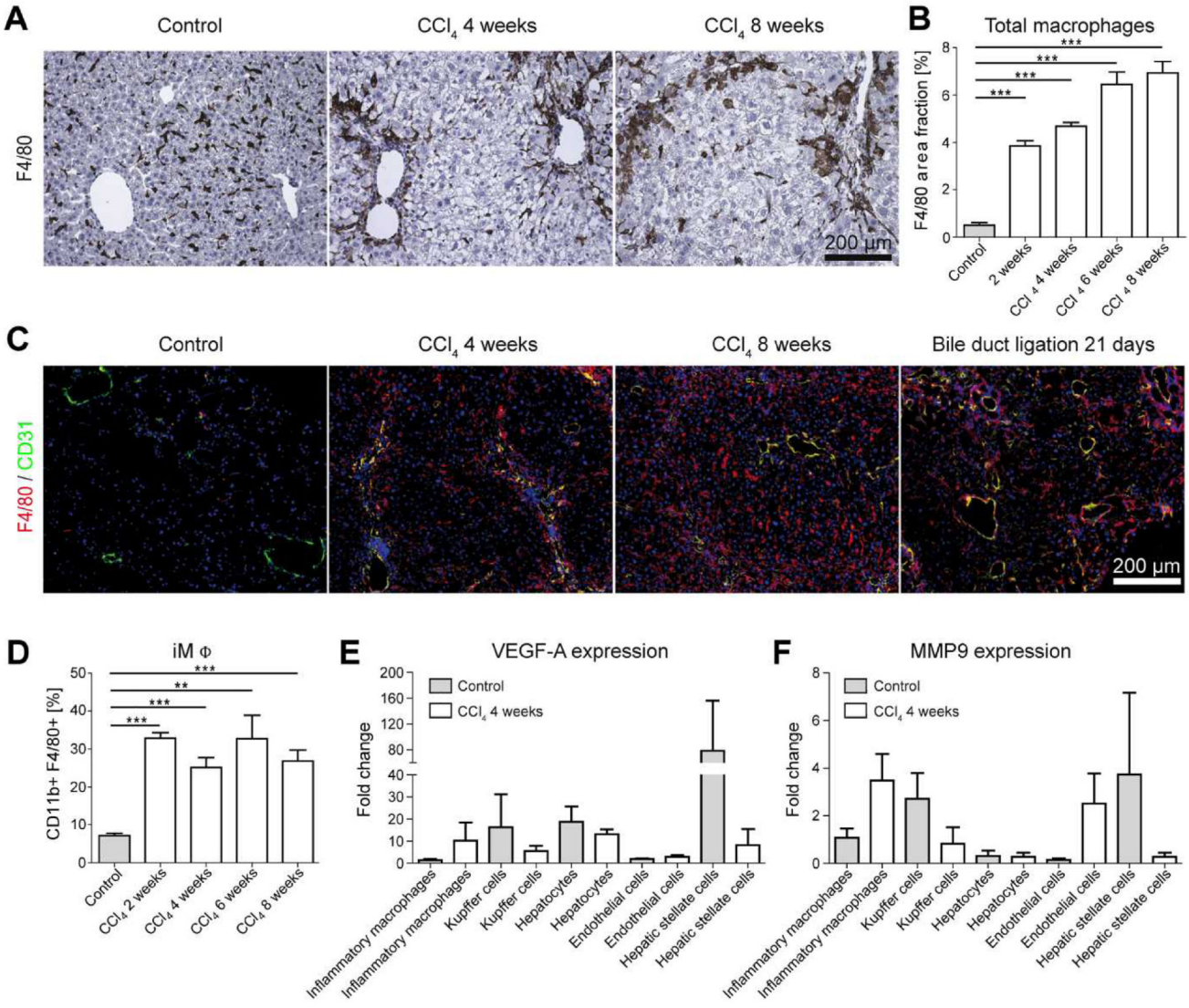

Figure 4. Role of hepatic macrophage subsets in fibrosis-associated angiogenesis

Chronic toxic liver injury was induced by repetitive i.p. administrations of CCl_4 in c57BL/6 mice, control mice received corn oil. Mice were sacrificed 48 hours after the last injection of CCl_4 (n=6 mice per condition and time-point). (A) Representative microscopy images of F4/80 immunohistochemistry (macrophages). (B) Quantification of total $F4/80^+$ macrophages in sections from control and chronically injured livers. (C) Representative F4/80 (red) and CD31 (green) co-stainings, demonstrating periportal localization of inflammatory macrophages and co-localization of macrophages with newly formed small blood vessels in progressive CCl_4 or BDL injury. (D) The relative amount of intrahepatic $CD11b^+$ $F4/80^+$ inflammatory macrophages (iMΦ) isolated by FACS sorting is early and persistently increased in chronic liver injury. (E+F) Expression of VEGF-A (E) and MMP9 (F) by primary murine inflammatory macrophages, Kupffer cells, hepatocytes, endothelial cells and hepatic stellate cells. Cells were isolated from injured (n=12) and control (n=12) livers using FACS sorting, and expression levels were normalized to iMΦ isolated from corn

oil-treated control livers. Data are shown as mean±SD. ***$P<0.001$ and **$P<0.01$ (Student's t test).

Europe PMC Funders Author Manuscripts

Europe PMC Funders Author Manuscripts

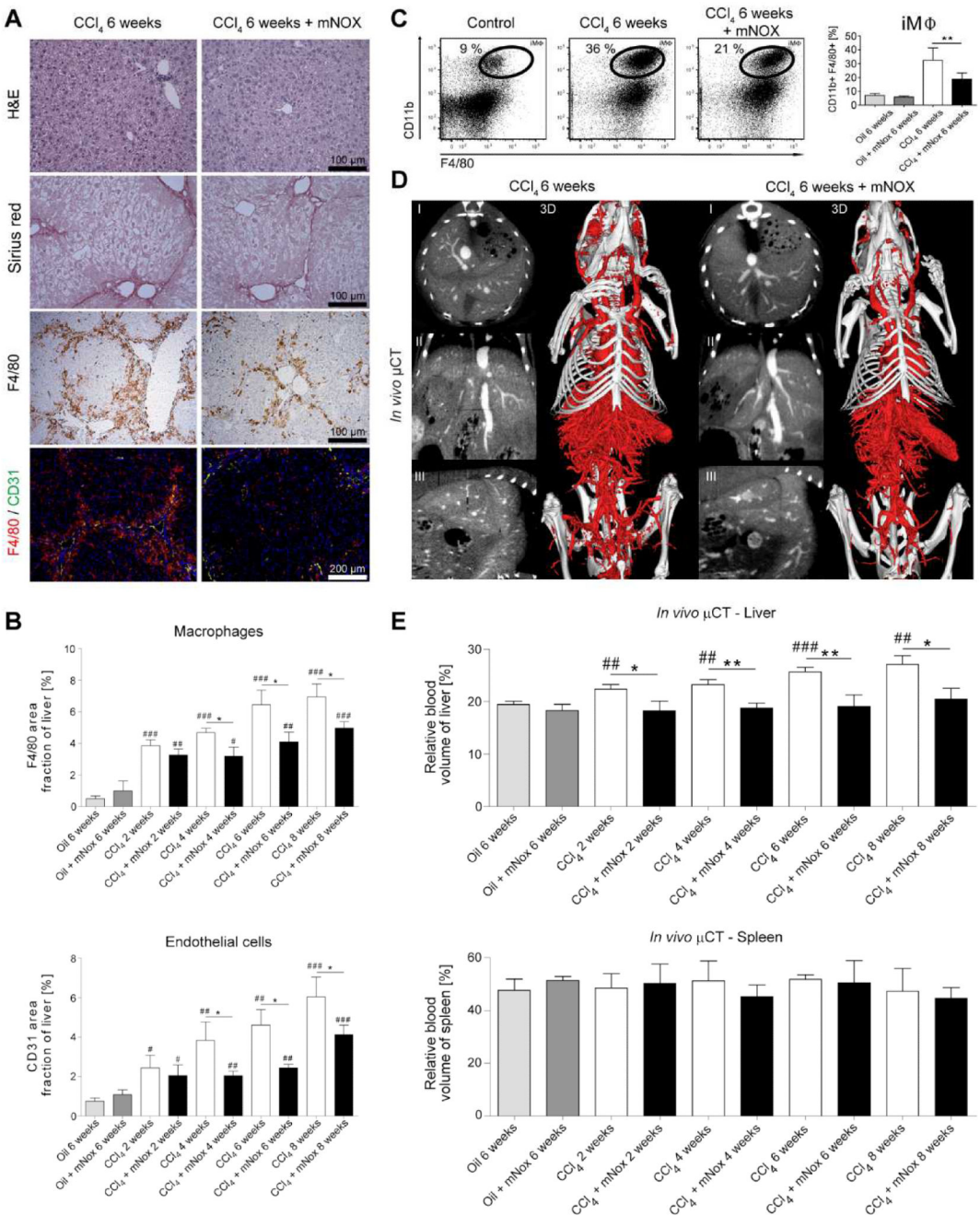

Figure 5. Effect of pharmacological inhibition of CCL2-dependent inflammatory monocytes on fibrosis-associated angiogenesis

Chronic toxic liver injury was induced by repetitive i.p. administrations of CCl_4 in c57BL/6 mice, and half of these animals received thrice weekly s.c. injections of the specific CCL2 inhibitor mNOX-E36, to block the CCL2-dependent infiltration of inflammatory monocytes. Analyses were performed 48 hours after the last CCl_4 injection. Control mice received corn oil for 6 weeks. (A) Representative H&E staining, Sirius red, F4/80 immunohistochemistry, and F4/80-CD31 immunofluorescence co-stainings. (B) Quantification of $F4/80^+$ macrophages and $CD31^+$ blood vessels in livers of chronically injured and mNOX-E36

Europe PMC Funders Author Manuscripts

treated mice. (C) Representative FACS plots and statistical analysis showing the increase of intrahepatic inflammatory macrophages (iMΦ) in chronically injured livers and their significant reduction in mNOX-E36 treated livers. iMΦ were separated from Kupffer cells on the basis of differential expression of F4/80 and CD11b. (D) Liver vascularization visualized by contrast-enhanced *in vivo* μCT. (E) Quantification of the rBV in livers and spleens using functional *in vivo* μCT imaging. Data are shown as mean±SD. ***P<0.001, **P<0.01 and *P<0.05 for comparing CCl_4 vs. CCl_4+mNOX-E36; ###P<0.001, ##P<0.01 and #P<0.05 for comparing CCl_4 or CCl_4+mNOX-E36 vs. corresponding control groups (i.e. 6 weeks oil or 6 weeks oil+mNOX-E36) (n=30 mice; Student's *t* test).

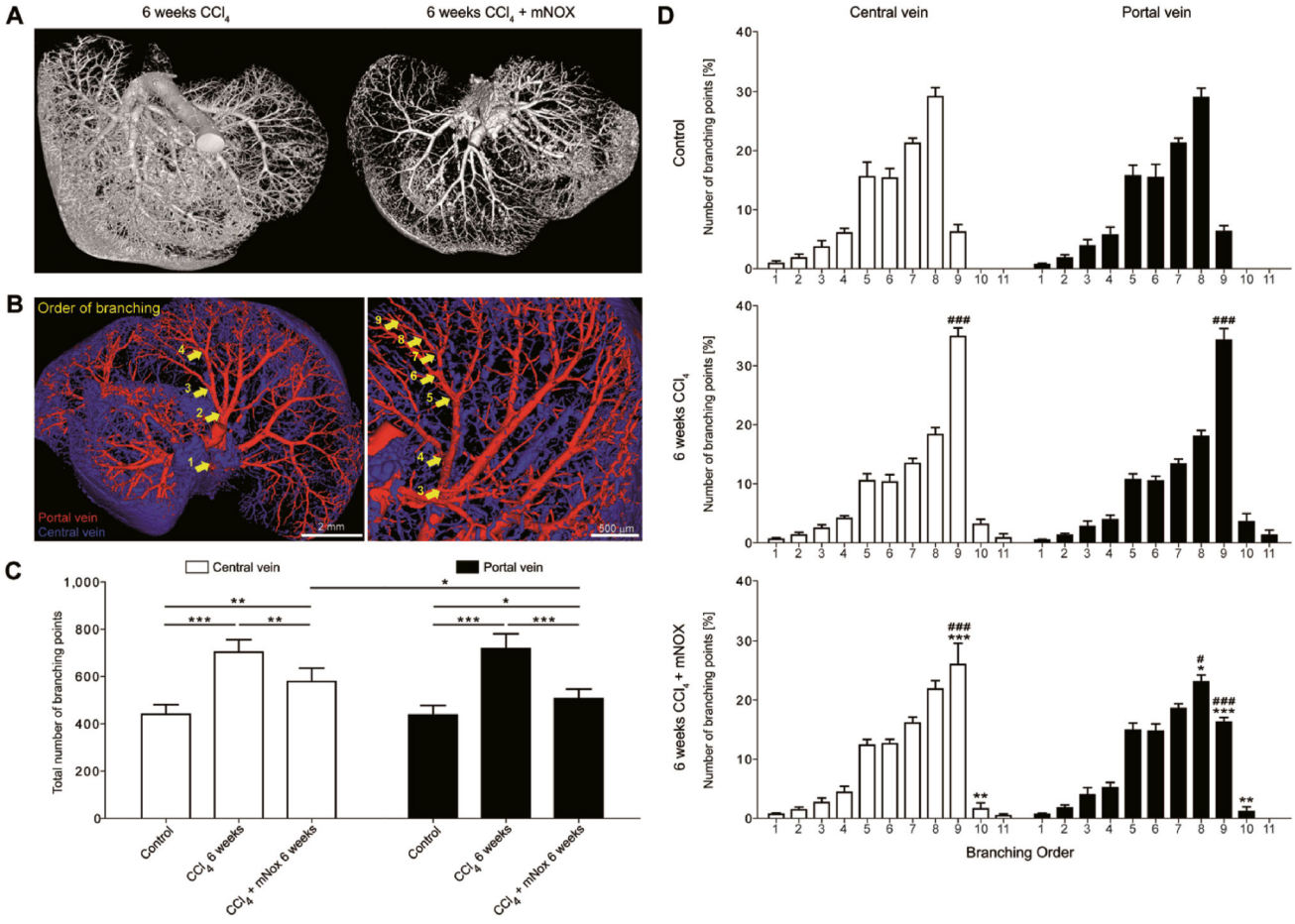

Figure 6. Vascular branching analysis of sprouting angiogenesis in the central and portal vein system in progressive liver fibrosis and upon pharmacological inhibition of CCL2

(A) Representative high-resolution *ex vivo* µCT images of chronically injured and mNOX-E36-treated livers after systematic Microfil perfusion. (B) Overview and magnification of segmented blood vessels of the liver after semi-automated discrimination between vessels related to the central (blue) or portal vein (red) system. Arrows schematically depict the order of rising branching points along the course of blood vessels, from center to periphery. (C) µCT-based quantification of the mean total number of branching points in livers from corn oil-, CCl_4- and CCl_4+mNOX-E36-treated mice (all for 6 weeks). Branching points from five representative blood vessels were quantified for both the central and the portal vein system. (D) µCT-based quantification of the percentage of branching points per increasing order (1st to 11th branching order) for livers from corn oil-, CCl_4- and CCl_4+mNOX-E36-treated mice. Data are shown as mean±SD. ***P<0.001, **P<0.005 and *P<0.05 (Student's t test) for comparing CCl_4 vs. CCl_4+mNOX-E36; ###P<0.001, and #P<0.05 for comparing CCl_4 or CCl_4+mNOX-E36 vs. control (Student's t test) (D).

Europe PMC Funders Author Manuscripts

Europe PMC Funders Author Manuscripts

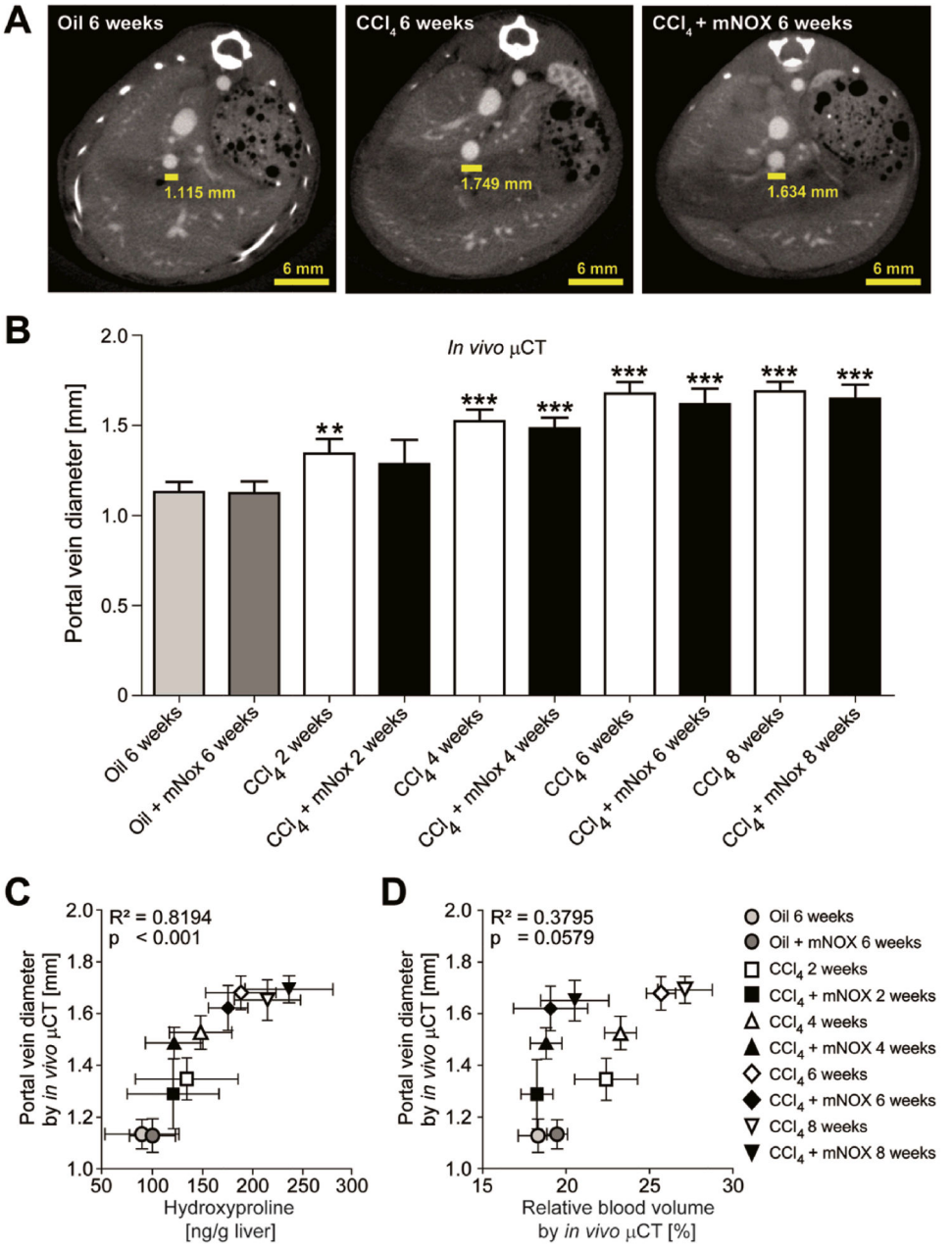

Figure 7. *In vivo* quantification of the portal vein diameter using contrast-enhanced µCT imaging

(A) Cross-sectional images in transversal planes exemplifying the determination of the portal vein diameter 3-4 slices above the junction of the superior mesenteric and splenic vein in control, chronically injured and mNOX-E36 treated livers. (B) Quantification of the portal vein diameter using functional µCT imaging in combination with an iodine-based large molecular weight blood pool contrast agent. (C) A highly significant correlation was found between *in vivo* quantified portal vein diameters and *ex vivo* determined hydroxyproline content. (D) No significant correlation was found for the comparison between portal vein diameters and relative blood volumes in CCl_4 treated, CCl_4 + mNOX-

E36 treated or control mice. Data are shown as mean±SD. ***P<0.001, **P<0.01 for comparing CCl_4 or mNOX-E36 vs. corresponding control groups (i.e. 6 weeks oil or 6 weeks oil + mNOX-E36) (n=30 mice; Student's *t* test).

Europe PMC Funders Author Manuscripts